IEEE Photonics Journal
An IEEE Photonics Society Publication

Open Access

Optimization of Timing Jitter Reduction by Optical Feedback for a Passively Mode-Locked Laser

Volume 6, Number 5, October 2014

C. Otto
L. C. Jaurigue
E. Schöll
K. Lüdge

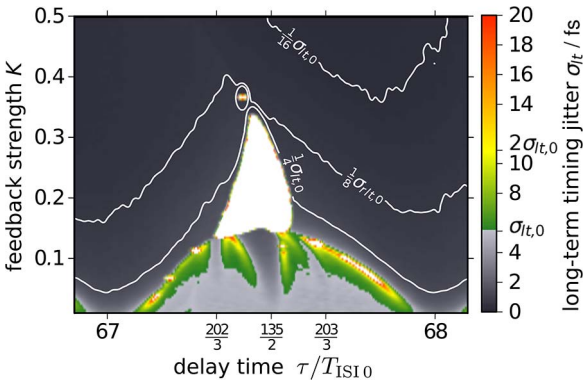

DOI: 10.1109/JPHOT.2014.2352934
1943-0655 © 2014 IEEE

IEEE photonics SOCIETY

IEEE

Optimization of Timing Jitter Reduction by Optical Feedback for a Passively Mode-Locked Laser

C. Otto,[1,2] L. C. Jaurigue,[1] E. Schöll,[1] and K. Lüdge[1]

[1]Institute of Theoretical Physics, Technical University of Berlin, 14195 Berlin, Germany
[2]Potsdam Institute for Climate Impact Research, 14473 Potsdam, Germany

DOI: 10.1109/JPHOT.2014.2352934

Manuscript received July 18, 2014; revised August 15, 2014; accepted August 18, 2014. Date of publication August 27, 2014; date of current version September 12, 2014. This work was supported by DFG in the framework of GRK 1558. Corresponding author: L. C. Jaurigue (e-mail: linajaurigue@mailbox.tu-berlin.de).

Abstract: We investigate the effect of optical self-feedback on the timing jitter of a passively mode-locked (ML) laser and compare the von Linde method with two pure time domain methods for calculating the timing jitter of such a system. We find that all three methods yield the same dependence of the timing jitter on the external cavity roundtrip time (delay time). Of these methods, the so-called long term jitter method is significantly less computationally expensive. We therefore use this method to investigate the influence of the delay time, feedback strength, and amplitude-phase coupling on the timing jitter. Our results show that, with vanishing amplitude-phase coupling, greater timing jitter reduction can be achieved with long delay times and larger feedback strengths, when feedback is near resonance. Off resonance, the timing jitter is increased. Non-vanishing amplitude-phase coupling can lead to destabilized pulse stream, even at the feedback main resonances.

Index Terms: Semiconductor lasers, laser mode locking, optical feedback.

1. Introduction

Mode-locked (ML) semiconductor lasers are of great interest as sources of high repetition rate ultrashort pulses. They have potential applications in a wide range of fields including data communication, high-speed optical sampling, optical clocking and microscopy [1]–[3]. Passively ML lasers are of particular interest as, compared with hybrid and actively ML lasers, they are easy to fabricate and to deal with in experiments [4]. However, they have the drawback of a relatively large timing jitter due to the absence of an external reference clock [5], [6]. Since precise pulse arrival times are desired for applications, a means of reducing the timing fluctuations is needed.

Research efforts to this end have demonstrated that optical feedback can have a stabilizing effect on the lasers dynamics, thereby reducing the timing jitter [7]–[9]. Optical feedback can, however, also have a destabilizing effect, depending on the feedback conditions [7], [10]. Therefore, to achieve optimal timing jitter reductions a comprehensive study of the affect of optical feedback is required. So far, only few theoretical works have been published on this topic, and of those works most have focused on the regimes of short to intermediate external cavity roundtrip times τ [11]–[13]. This will be in part due to the computational expense of the required calculations.

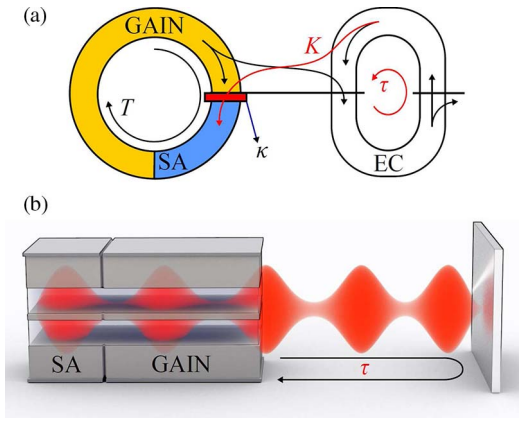

Fig. 1. (a) Diagram of the ring cavity laser coupled to an external feedback loop. The ring cavity consists of a gain section (GAIN), a saturable absorber (SA), and a Lorentzian filter (red bar). T and τ are the internal and external cavity roundtrip times, respectively, and K is the feedback strength. κ models the linear nonresonant losses per laser cavity roundtrip. (b) Diagram of a two section linear cavity Fabry-Perot ML laser subject to optical feedback. We aim to describe experiments using this type of laser with the DDE model.

In this study, and in [10] and [14], the computational cost of timing jitter calculations was reduced, compared with the aforementioned studies, by using a delay differential equation model as opposed to a finite-difference traveling wave model. Nevertheless, timing jitter calculations using standard methods are still very time consuming. In this paper we therefore compare different timing jitter calculation methods. We then investigate the influence of τ and the feedback strength on the timing jitter in the regimes of intermediate and long τ.

The paper has the following layout. In Section 2, the delay differential equation (DDE) model, with optical feedback, is described. Three methods of timing jitter calculation are then discussed in Section 3. The results of these timing jitter calculation methods are subsequently compared in Section 4. Here, the dependence of the timing jitter on the feedback delay time is also discussed. In Section 5, the impact of the feedback strength is discussed, as well as the dependence of the timing jitter on the linewidth enhancement factor (α-factor).

2. Delay Model for Mode-Locked Laser Subject to Optical Feedback

We use the DDE model for a passively mode-locked ring cavity laser subject to optical feedback, introduced in [10]. This model is an extension of the DDE model proposed in [15] and [16]. The system modeled is a ring cavity with an actively pumped gain section and a saturable absorber section (see Fig. 1). It is assumed that lasing is unidirectional and that the group velocity v is constant throughout the cavity. Optical feedback is included by out-coupling light to an external ring cavity. A detailed description and derivation of the model can be found in [10]. The final set of three coupled delay differential equations is

$$\gamma^{-1}\dot{\mathcal{E}}(t)+\mathcal{E}(t)=R(t-T)e^{-i\Delta\Omega T}\mathcal{E}(t-T)+\sum_{l=1}^{\infty}K_l e^{-ilC}R(t-T-l\tau)e^{-i\Delta\Omega(T+l\tau)}\mathcal{E}(t-T-l\tau)+D\xi(t) \quad (1)$$

$$\dot{G}(t)=J_g-\gamma_g G(t)-e^{-Q(t)}\left(e^{G(t)}-1\right)|\mathcal{E}(t)|^2 \quad (2)$$

$$\dot{Q}(t)=J_q-\gamma_q Q(t)-r_s e^{-Q(t)}\left(e^{Q(t)}-1\right)|\mathcal{E}(t)|^2 \quad (3)$$

with

$$R(t)\equiv\sqrt{\kappa}e^{\frac{1}{2}\left((1-i\alpha_g)G(t)-(1-i\alpha_q)Q(t)\right)} \quad (4)$$

TABLE 1

Parameter values used in numerical simulations

symbol	value	symbol	value
γ	$2.5ps^{-1}$	T	$25ps$
γ_g	$1ns^{-1}$	$T_{ISI,0}$	$1.015\,T$
γ_q	$75ns^{-1}$	α_g	0
r_s	25.0	α_q	0
J_g	$4.8ps^{-1}$	$\Delta\Omega_0$	0
J_q	$2.5ps^{-1}$	C	0
κ	0.1	l	1
κ_2	1		

where the dynamical variables are the slowly varying electric field amplitude $\mathcal{E}$, the saturable gain G, and the saturable loss Q. The two delay times in this system are the cold cavity roundtrip time T and the external cavity roundtrip time (delay time) τ. The cold cavity round trip time is defined as $T \equiv v/L$, where L is the length of the ring cavity. The bandwidth of the laser is limited by the finite width of the gain spectrum, which is taken into account by a Lorentzian-shaped filter function with full-width at half maximum γ. The possibility of detuning between the frequency of the maximum of the gain spectrum and the frequency of the nearest cavity mode is allowed for by the inclusion of $\Delta\Omega$. The optical feedback is described by the sum in (1). Here, l is the number of roundtrips in the external cavity, K_l is the roundtrip dependent feedback strength and C is the phase of the light due to one roundtrip in the external cavity. The last term in (1) models spontaneous emission noise using a complex Gaussian white noise term $\xi(t)$ with strength D. The saturable gain G and saturable loss Q are related to the carrier inversion in the gain and absorber sections, respectively. In (2), J_g is proportional to the current pumped into the gain section and J_q in (3) is related to the carrier losses due to the reverse bias applied to the absorber section. The carrier lifetimes in the gain and absorber sections are given by $1/\gamma_g$ and $1/\gamma_q$, respectively. The factor r_s is proportional to the ratio of the saturation energies in the gain and absorber sections. Equation (4) describes the amplification and losses of the electric field during one roundtrip in the ring cavity. Internal and out-coupling losses are taken into account in the attenuation factor κ and the linewidth enhancement factor (α-factor) in the gain and absorber sections are denoted α_g and α_q, respectively.

A detailed description of the dynamics of this system is given in [10] and [17]. Important for the study of the timing jitter is the feedback resonance condition

$$p\tau = qT_{ISI,0}, \quad \text{for} \quad p, q \in \mathbb{N} \tag{5}$$

where $T_{ISI,0}$ is the interspike time interval between pulses for the solitary laser.

In the following we assume zero detuning, $\Delta\Omega = 0$. We also neglect all feedback contributions arising from multiple external cavity roundtrips $(l > 1)$ and define $K \equiv K_1$. To validate this simplification we assume the feedback to be small. Table 1 lists the parameter values used in the simulations.

3. Comparison of Timing Jitter Calculation Methods

Timing jitter is the deviation of a periodic signal from an ideal clock and can be calculated using various methods. The von Linde method [18] is commonly used in experiments [19]–[22]. This method uses the power spectral density (PSD) to calculate the root-mean-squared (rms) timing jitter. For the modeling of passively mode-locked lasers it, however, has several drawbacks. Firstly, Fourier transforms of the time series of $|\mathcal{E}|$ have to be calculated, which are computationally very expensive, limiting the frequency resolution that can be achieved. Secondly, strictly speaking it is only valid for stationary stochastic processes. For passively mode-locked lasers, the variance of the timing fluctuations increases with time, indicating a non-stationary stochastic

process [23]. Due to these drawbacks it is instructive to look to other methods of calculating the rms timing jitter. In [11] a pure time domain method was proposed. This method uses the power spectra of the timing fluctuations to calculate the rms timing jitter, which permits a better frequency resolution with less computational effort. (The timing fluctuations are the deviations of the interspike interval times T_{ISI} from the average roundtrip time of the light pulses in the laser cavity.) The idea behind the third method we investigate here is to assume that to a good approximation the timing fluctuations of a passively ML laser can be described by a random walk. This will be shown in Section 3.3. Under this assumption, the Fourier transform may be calculated analytically, and therefore the rms timing jitter can be calculated directly from the variance of the timing fluctuations [24]. The pure time domain methods also have the advantage that the timing jitter is calculated from only the timing positions of the pulses and therefore, assuming the pulse shape does not vary, the calculations are not influenced by amplitude modulations.

In the subsequent subsections the three methods mentioned above will be described. Following this we compare calculations of the timing jitter of the mode-locked laser subject to feedback, using these three methods. Finally we will use the timing jitter calculations to make predictions on optimal feedback conditions.

3.1 von Linde Method

The power spectrum of an ideal semiconductor ML laser consists of δ-peaks at the multiples $h\nu_{rep}$ $(h \in \mathbb{N})$ of the repetition rate of the pulses ν_{rep}. When noise is introduced these peaks broaden. Both the amplitude jitter and the timing jitter contribute to the broadening of these peaks. The von Linde method calculates the rms timing jitter from the PSD of the laser output, assuming that amplitude and timing fluctuations are uncorrelated and have stationary Gaussian probability distributions. Using the von Linde method the rms timing jitter is given by

$$\sigma_{rms}(\nu_{low}, \nu_{high}, N) \equiv \frac{T_C}{2\pi h} \sqrt{\int_{\nu_{low}}^{\nu_{high}} 2S_\varphi(\nu, N, h)\, d\nu} \tag{6}$$

where

$$S_\varphi(\nu, N, h) \equiv \frac{S_{|\mathcal{E}|}(\nu, N)}{P(h, N)} \tag{7}$$

is the phase noise PSD, and

$$T_C \equiv \left\langle \frac{1}{\tilde{N} - 1} \sum_{n=1}^{\tilde{N}-1} T_{ISI,n} \right\rangle_M \tag{8}$$

is the interspike interval averaged first over $\tilde{N}$ roundtrips for one noise realization and then averaged over M noise realizations. (In the case of active or hybrid ML T_C is the repetition period of the external modulation.) The integral is over the sidebands of the h-th harmonic of ν_{rep} starting from a small offset frequency from the peak ν_{low} and extending to ν_{high}. $S_{|\mathcal{E}|}(\nu, N)$ is the PSD of a discrete time series and $P(h, N)$ is the power of the h-th harmonic. For nonstationary processes $S_{|\mathcal{E}|}(\nu, N)$ and $P(h, N)$ depend on the integration time $T_i = Ndt$, where dt is the time step (sampling rate), and N is the number of steps. Von der Linde also derived that amplitude noise is independent of the number of the harmonic h, whereas the timing noise scales with h^2 [18]. The relative contribution of the timing is therefore greater at higher harmonics.

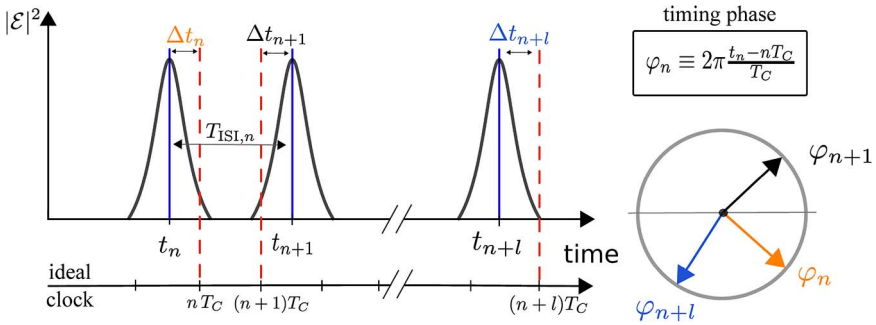

Fig. 2. Timing positions of the noisy pulse stream and their representation as phase oscillations.

3.2 Time Domain Power Spectral Density Method

Based on the pulse detection method described in [11] we use the following algorithm to detect the timing positions of the pulses: We define a probability density

$$\rho_n(t) \equiv \frac{\mathcal{G}^2(t)}{\mathcal{G}_n}, \quad \text{with} \quad \mathcal{G}_n \equiv \int_{t_{n,b}}^{t_{n,e}} \mathcal{G}^2(t)\, dt \tag{9}$$

using the net gain $\mathcal{G} \equiv G - (Q - |\ln\kappa|)$, where $t_{n,b}$ ($t_{n,e}$) is the first time point at which the leading (trailing) edge of the n-th pulse exceeds (falls below) a threshold $\mathcal{G}(t_{n,b}) > \mathcal{G}_{thres}$ ($\mathcal{G}(t_{n,e}) < \mathcal{G}_{thres}$). The timing position of the n-th pulse is then given by

$$t_n \equiv \int_{t_{n,b}}^{t_{n,e}} \rho_n(t)\, t\, dt. \tag{10}$$

This detection method is based on the observation that the main pulse is shaped by a net gain window (see [10] for details). Only the main pulses can be detected using this method, not the smaller feedback induced pulses as these are not large enough to open a net gain window. In the main resonance regime this method is exact as there is only one pulse in the cavity.

For each of the M noise realizations, a set of timing fluctuations is obtained

$$\{\Delta t_n \equiv t_n - nT_C\}_{n=1}^{N} \tag{11}$$

which are the deviations of the pulse arrival times $\{t_n\}_{n=1}^{N}$ from the arrival times of the pulses for an ideal jitter free pulse stream, $\{nT_C\}_{n=1}^{N}$ (see Fig. 2). For the clock time T_C the average of the interspike interval over the M noise realizations is used.

The rms timing jitter can then be calculated from the power spectral density of the timing fluctuations $S_{\Delta t}(\nu, N)$ using

$$\sigma_{rms}(\nu_{low}, \nu_{high}, N) \equiv \sqrt{\int_{\nu_{low}}^{\nu_{high}} 2S_{\Delta t}(\nu, N)\, d\nu} \tag{12}$$

where N is the number of timing fluctuations and hence indicates the length of the integration time $T_i = N\, dt$, and ν_{low} and ν_{high} are the minimal and maximal offset from the ideal repetition rate $1/T_C$, respectively.

The PSD of the timing fluctuations can be related to the phase noise spectral density introduced earlier (see (7)). This is done by expressing the timing fluctuations as a set of timing phase fluctuations

$$\left\{\varphi_n \equiv \frac{2\pi}{T_C}\Delta t_n = 2\pi\frac{t_n - nT_C}{T_C}\right\}_{n=1}^{N} \tag{13}$$

(see Fig. 2). Considering the timing phase as a continuous variable of time $\varphi = \varphi(t)$ with $\varphi(t_k) = \varphi_k$, it becomes obvious that the power spectra of the timing fluctuations and of the phase fluctuations are related by

$$S_\varphi(\nu_{off}, N) = \left(\frac{2\pi}{T_C}\right)^2 S_{\Delta t}(\nu_{off}, N). \tag{14}$$

The PSD of the phase fluctuations corresponds to (7) with $h = 1$. For non-stationary stochastic processes, the power spectra depend on the number N of timing fluctuations, i.e., on the length T_i of the time series. Experimentally, the noise of the timing phase is obtained by the noise of the lowest harmonics $(h = 1)$ of the output of a photodiode measuring the intensity of the ML laser, i.e., from the noise of the photocurrent [25], and corresponds to the phase noise introduced in Section 3.1.

The instantaneous repetition frequency of the pulses ν_{rep} is given by the derivative of φ with respect to time

$$\nu_{rep}(t) = \frac{d\varphi(t)}{dt}. \tag{15}$$

Taking into account that the Fourier transform of the linear operator d/dt yields a multiplication with $2\pi\nu$, the PSD of the timing phase can be expressed in terms of the PSD $S_{\nu_{rep}}$ of the repetition frequency ν_{rep} as

$$S_\varphi(\nu, N) = \frac{1}{\nu^2} S_{\nu_{rep}}(\nu, N). \tag{16}$$

Thus, fluctuations of low (offset) frequencies ν lead to larger accumulated timing deviations, i.e., larger fluctuations of the timing phase. Furthermore, if $S_{\nu_{rep}}$ is frequency independent, i.e. the noise of ν_{rep} is white, $S_\varphi \propto 1/\nu^2$.

3.3 Long-Term Timing Jitter Method

Fig. 3 shows the dependence of the variance

$$\mathrm{Var}(\Delta t_n)(n, \tau) \equiv \left\langle (\Delta t_n(\tau))^2 \right\rangle_M \tag{17}$$

of the timing fluctuations on the number of roundtrips n in the ring cavity for several external cavity delay times. After about 5000 roundtrips the variance appears to depend linearly on the roundtrip number. Since $\mathrm{Var}(\Delta t)/n$ is a constant for large n, it is a good measure of the timing jitter

$$\sigma_{lt} \equiv \sqrt{\frac{\mathrm{Var}(\Delta t_n)}{n}}. \tag{18}$$

This type of jitter is know as long-term timing jitter [24].

As the variance depends linearly on the roundtrip number, and hence time, the timing fluctuations can be described by a random walk with diffusion constant σ_{lt}. Due to this, by calculating

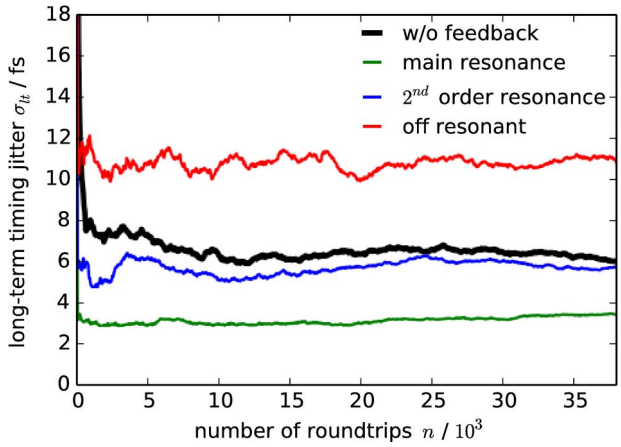

Fig. 3. Long-term jitter σ_{lt} as a function of the number of roundtrips n of the light in the internal cavity for the solitary laser (black line), the main resonance with $\tau = 7\ T_{ISI,0}$ (green line), the second order resonance with $2\tau = 15\ T_{ISI,0}$ (blue line) and for the non-resonant case with $\tau = 7.22\ T_{ISI,0}$ (red line). Parameters: $D = 0.2$, $K = 0.1$, and the other parameter as in Table 1.

the autocorrelation of the timing deviations and using the Wiener-Khinchin theorem [23], it can be shown that the PSD of the timing fluctuations is related to σ_{lt} by

$$S_{\Delta t}(\nu, T_i) = \frac{\sigma_{lt}^2}{2\pi^2 T_C \nu^2}\left[1 - \frac{\sin(2\pi\nu T_i)}{\nu T_i}\right] \overset{2\pi\nu T_i \gg 1}{\approx} \frac{\sigma_{lt}^2}{2\pi^2 T_C \nu^2} \tag{19}$$

where T_i is the integration time (derivation shown in [17]). In the limit of long integration times $\nu T_i \gg 1$ the second term in the rectangular brackets vanishes and the remaining term shows the $1/(\nu^2)$ dependence of $S_{\Delta t}$ (and thus of S_φ) indicating that in this approximation the noise of ν_{rep} is white (see Eq. (16)). The rms timing jitter can then be related to the long-term jitter using expression (19). The rms timing jitter then reads

$$\begin{aligned}\sigma_{rms}(\nu_{low}, \nu_{high}, T_i) &= \sqrt{\int_{\nu_{low}}^{\nu_{high}} 2S_{\Delta t}(\nu, T_i)\, d\nu} \\ &= \frac{\sigma_{lt}}{\pi\sqrt{T_C}}\sqrt{\left(\frac{1}{\nu_{low}} - \frac{1}{\nu_{high}}\right)} \approx \frac{\sigma_{lt}}{\pi\sqrt{T_C}}\frac{1}{\sqrt{\nu_{low}}}.\end{aligned} \tag{20}$$

The above equation reveals that in the limit in which the timing fluctuations can be described by a random walk, σ_{rms} and σ_{lt} differ only by a constant, which depends on the lower integration boundary ν_{low} and on the ideal pulse repetition time T_c.

4. Dependence of rms Timing Jitter and the Long-Term Timing Jitter on Feedback Strength and External Cavity Length

In this section, the dependences of the rms and long-term timing jitter on the feedback delay are discussed and compared. We consider two feedback regimes, one with an intermediate delay time and the other with a long external delay time. In all simulations the system of DDEs in (1)–(3) was first integrated for a sufficiently long time before calculating the timing jitter such that any transient behavior is avoided.

As is highlighted by the description of the von Linde method in the previous section, information on the timing jitter can be obtained from the PSD of the absolute value of the electric field amplitude $|\mathcal{E}|$. Fig. 4(a) shows PSD of $|\mathcal{E}|$ for a range of intermediate delay times. The spectra are centered about the 25th harmonic of the fundamental mode-locking frequency of the solitary

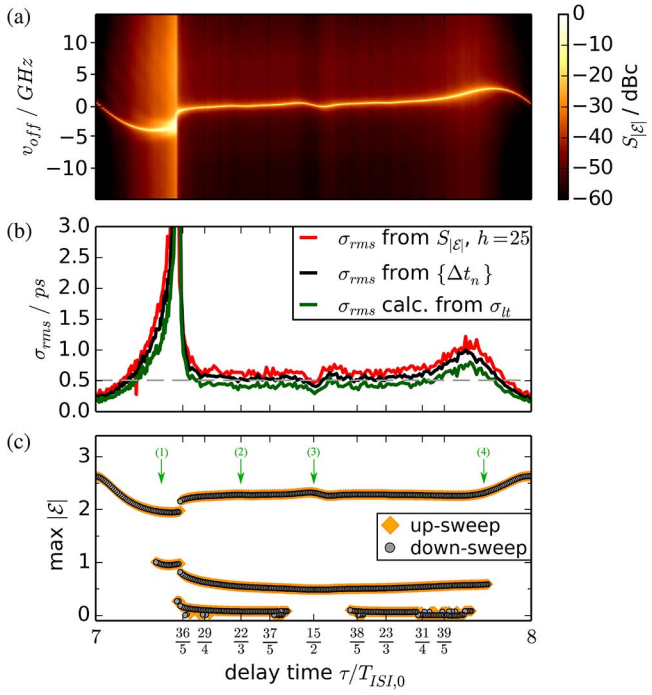

Fig. 4. (a) PSD of the absolute value of the field amplitude $|\mathcal{E}|$ versus the delay time τ for intermediate delay and small feedback strength $K = 0.1$. The spectra are centered at the $h = 25$th harmonic and $\nu_{off} = \nu - h\nu_{rep}$ is the off-set frequency from the 25th harmonic of the free running laser $25\nu_{rep}$. (b) Root-mean-square timing jitter σ_{rms} versus τ. Depicted in red is σ_{rms} calculated from the power spectra of $|\mathcal{E}|$ (see (6)), in black is σ_{rms} calculated from the power spectra of the timing fluctuations $\{\Delta t_n\}$ (see (12)) and in green is σ_{rms} calculated from the long-term timing jitter σ_{lt} (see (2)). The dashed gray line indicates the timing jitter of the solitary laser. (c) Bifurcation diagram of the maxima of $|\mathcal{E}|$ versus τ for up-sweeping (orange diamonds) and down-sweeping (grey dots) τ, for the deterministic system $(D = 0)$. Parameters: $T_i = 4 \cdot 10^4$ $T_{ISI,0}$, $D = 0.2$, $K = 0.1$, and other parameters as in Table 1.

laser. Such a high harmonic is used to minimize the influence of amplitude modulations. The delay time is given in units of the solitary laser interspike interval time $T_{ISI,0}$ and extends from the seventh main resonance to the eighth. Here, it can be seen that the sidebands are lowest in the main resonance regions, indicating a lower timing jitter than in the non-resonant regimes. Comparatively lower sidebands can also be observed at higher order resonances, such as at $\tau = 15/2$. The frequency position of the peak power for each delay time indicates the repetition rate. Therefore, tracing the position of the peak power the frequency pulling of the repetition rate can be observed. This effect is discussed in detail in [10].

Fig. 4(b) shows the rms timing jitter plotted against the delay time for the three jitter calculation methods discussed in the previous section. All three methods produce the same dependence on the delay time and comparing with the power spectra in Fig. 4(a) σ_{rms} shows the expected trends. Near the main resonances the timing jitter is reduced with respect to the solitary laser. A reduction with respect the solitary laser is also observed at the 2nd order resonance $\tau/T_{ISI,0} = 15/2$. Just below $\tau/T_{ISI,0} = 36/5$ non-resonant feedback greatly increases the timing jitter. This increase corresponds to the high power side bands observed in Fig. 4(a).

A second area of increased timing jitter is observed just before the eighth main resonance. Comparing with the bifurcation diagram shown in Fig. 4(c) we see that the regions of large timing jitter correspond to significant changes in the output of the deterministic system. The bifurcation diagram shows the maximum of the absolute value of the electric field as a function of τ, once for up-sweeping τ (orange diamonds) and once for down-sweeping τ (grey dots). Near $\tau/T_{ISI,0} = 36/5$, there is a bistability between the two solution paths. This bistability coincides with the large timing jitter observed in Fig. 4(a). At this bistability switching events between the

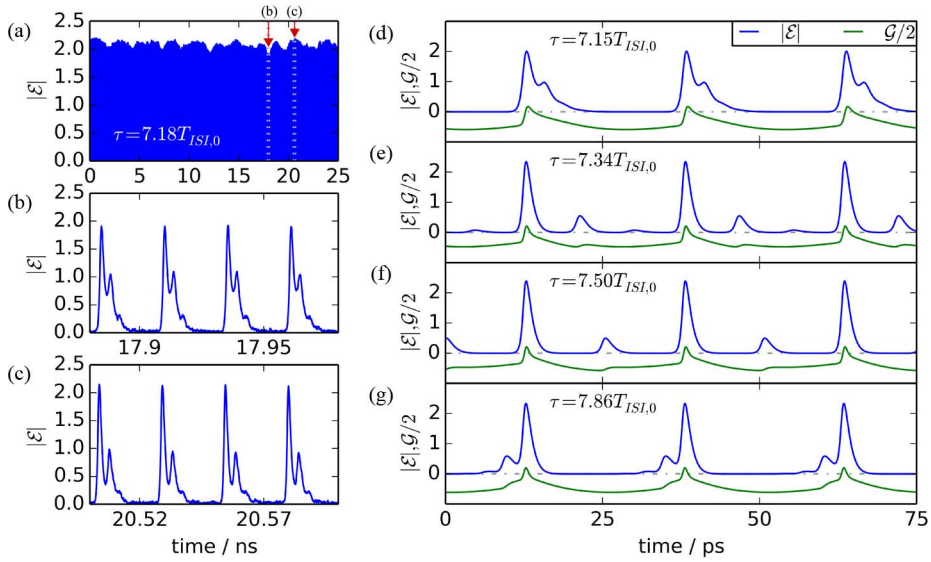

Fig. 5. (a) Timeseries of the absolute value of the field amplitude $|\mathcal{E}|$ for the system with noise $(D = 0.2)$ for $\tau = 7.17\ T_{ISI,0}$. Panels (b) and (c) show close-ups of the regions marked by dotted lines in panel (e). (d)–(g) Timeseries of the absolute value of the field amplitude $|\mathcal{E}|$ and the net gain $\mathcal{G}$ for the deterministic system $(D = 0)$ for $\tau = 7.15\ T_{ISI,0}$ (Fig. 4 arrow (1)), $\tau = 7.34\ T_{ISI,0}$ (Fig. 4 arrow (2)), $\tau = 7.50\ T_{ISI,0}$ (Fig. 4 arrow (3)), and $\tau = 7.86\ T_{ISI,0}$ (Fig. 4 arrow (4)). Parameters: $K = 0.1$ and other parameters as in Table 1.

two deterministic solutions can be observed. This is shown in the timeseries depicted in Fig. 5(a)–(c). The panel (a) shows a timeseries of $|\mathcal{E}|$ over many roundtrips. Changes in the peak height indicate switching between the two solutions. The panels (b) and (c) show close-ups of regions where the system exhibits different solutions.

The increase of the timing jitter, with respect to the solitary laser, in regions where no bistability is observed can be understood by looking at the output of the deterministic system in these regions. Fig. 5(d)–(g) shows timeseries of $|\mathcal{E}|$ and the net gain for several values of the external delay time. For external delay times that give rise to an increased timing jitter the deterministic system displays deformed, or multiple peak pulses and the net gain is larger over a slightly greater time window. This makes the system less stable to random fluctuations. In (e) and (f) of Fig. 5 multiple pulses are observed, however these are well separated within the ring cavity and therefore do not corresponds to regions of increased timing jitter in the system with noise.

In Fig. 6, the same plots are shown as in Fig. 4, except in the regime of long delay instead of intermediate delay. Comparing plots (a) of Figs. 4 and 6 one can see that for longer delay the area of resonant feedback extends over a larger range of τ values about the main resonance. This is shown by the areas with low power sidebands. In [14] a much longer feedback cavity was simulated and the resonance regions were found to extend from one main resonance to the next. This is consistent with the trend observed here. In Fig. 6(b) all rms timing jitter calculations show the same τ dependent trends. These are also in agreement with the trends indicated by the power spectra in Fig. 6(a). Comparing Fig. 6(b) with Fig. 4(b) shows that for longer delay times there is a greater timing jitter reduction with resonant feedback. Off resonance, the timing jitter is also increased (with respect to the solitary laser) in the longer delay regime. In this delay regime no switching events were observed in regions of bistability. Here, it is instructive to look to the output of the deterministic system to understand the increase of the timing jitter. Fig. 7 shows time series of $|\mathcal{E}|$ and $\mathcal{G}$ for several τ values. Once again, regions of increased timing jitter correspond to deformed pulses in the deterministic system and slight decreases in the timing jitter at higher order resonances correspond to multiple well-separated pulses within the ring cavity. In panel (d) of Fig. 7 (corresponding to the delay for which the largest timing jitter is observed in Fig. 6(b)) a plateau of $\mathcal{G}$ close to zero can clearly be seen. This indicates that for

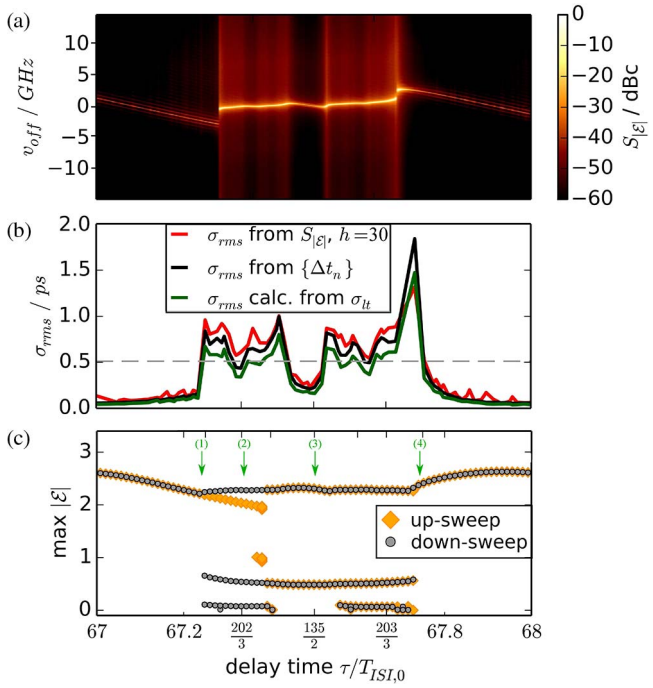

Fig. 6. Same as in Fig. 4 but in the regime of long delay times τ.

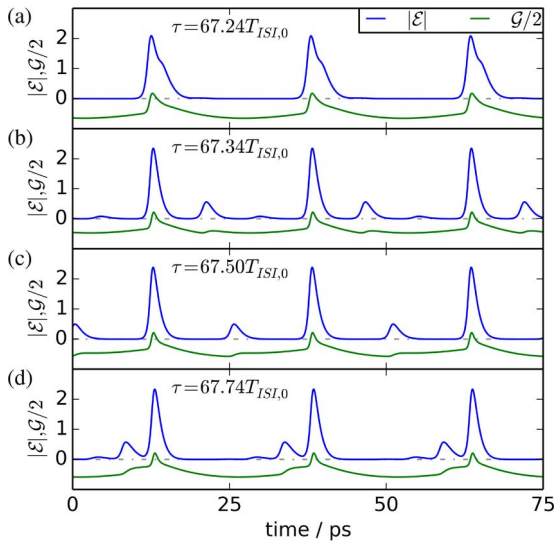

Fig. 7. Timeseries of the absolute value of the field amplitude $|\mathcal{E}|$ and the net gain $\mathcal{G}$ for the deterministic system for $\tau = 67.24T_{ISI,0}$ (Fig. 6 arrow (1)), $\tau = 67.34T_{ISI,0}$ (Fig. 6 arrow (2)), $\tau = 67.50T_{ISI,0}$ (Fig. 6 arrow (3)), and $\tau = 67.74T_{ISI,0}$ (Fig. 6 arrow (4)). Parameters: $K = 0.1$, $D = 0$, and other parameters as inTable 1.

this delay $(\tau = 67.74T_{ISI,0})$, the system is particularly susceptible to noise fluctuations, as these could open a net gain window $(\mathcal{G} > 0)$.

In [14], it is reported that for some feedback cavity lengths they obtained different interspike interval times for different noise realizations. We have also observed such effects, however at larger feedback strengths. As this leads to erroneously higher timing jitter values, we have chosen the initial conditions such that all noise realizations land on the same solution. In [14], this

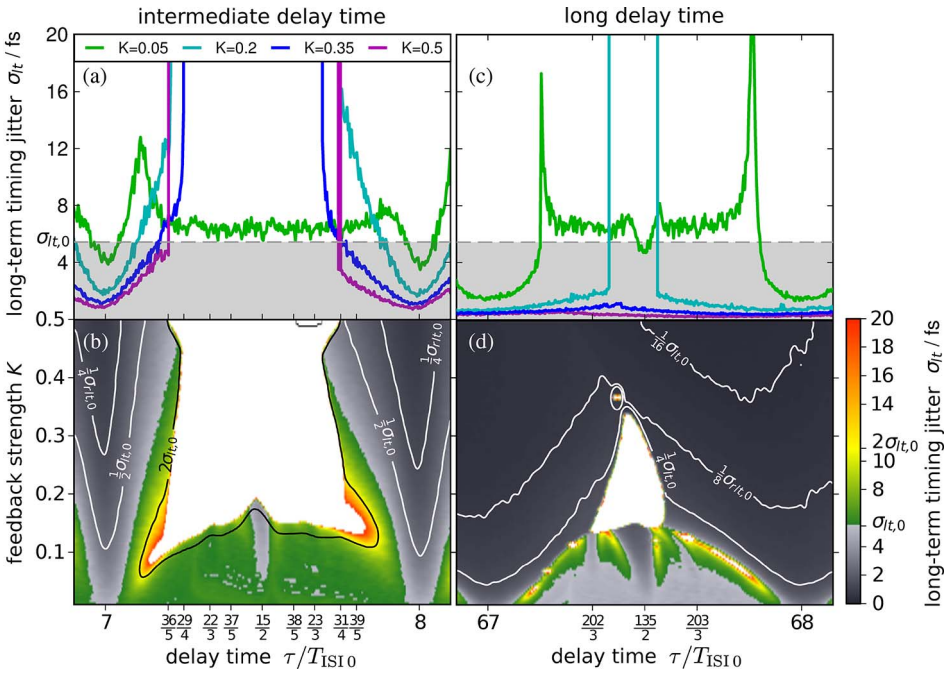

Fig. 8. Long-term timing jitter σ_{lt} as a function of the delay time τ and the feedback strength K for intermediate delay (b) and long delay (d). The gray-scale denotes a reduction of σ_{lt} with respect to $\sigma_{lt,0}$ and the green to red color scale indicates an enhancement of σ_{lt} with respect to $\sigma_{lt,0}$. The white regions indicate unstable pulse trains. Cuts at various feedback strengths are shown in (a) and (b) for intermediate and long delay times, respectively. Parameters: $T_i = 4 \cdot 10^4$ $T_{ISI,0}$, $D = 0.2$, $K = 0.1$, and other parameters as in Table 1.

is observed at lower feedback strengths because they simulate a longer cavity, therefore there are more stable solutions to the system of DDEs. This effect is not to be confused with the switching between solutions within one realization which is discussed above.

Although all three timing jitter calculation methods show the same τ dependence in Figs. 4(b) and 6(b), the magnitude of σ_{rms} calculated using the von Linde method is generally slightly higher. However, as we are primarily interested in the relative timing jitter this is not important. From these plots we can also conclude that the exclusion of the smaller feedback-induced pulses, from the pulse detection method used for the two time domain calculation methods, has only a negligible effect.

5. Dependence of Timing Jitter on Feedback Strength and α-Factor

Having found that the long-term timing jitter exhibits the same τ dependence as the timing jitter calculated using the von Linde method we can use the much less time consuming long-term jitter calculation to investigate the dependence of the timing jitter on the feedback strength and on the α-factors of the gain and absorber sections. In Fig. 8(b) and (d), σ_{lt} is plotted as a function of feedback strength and delay time, for intermediate and long delay, respectively. The gray-scale denotes a reduction of σ_{lt} with respect to $\sigma_{lt,0}$ and the green to red color scale indicates an enhancement of σ_{lt} with respect to $\sigma_{lt,0}$. White regions indicate unstable pulse streams, here the periodic pulse train of the free running laser is destabilized by the feedback leading to a non-periodic behavior and very large timing jitter values. Fig. 8(a) and (c) depict σ_{lt} versus the delay time at selected feedback strengths, for intermediate and long delay, respectively. For all plots in Fig. 8 $\alpha_g = \alpha_q = 0$. These plots show that there is a resonance cone about the main resonances, the width of which increases with the increasing feedback strength. For intermediate delay the pulse stream is destabilized for large feedback strengths away from the main

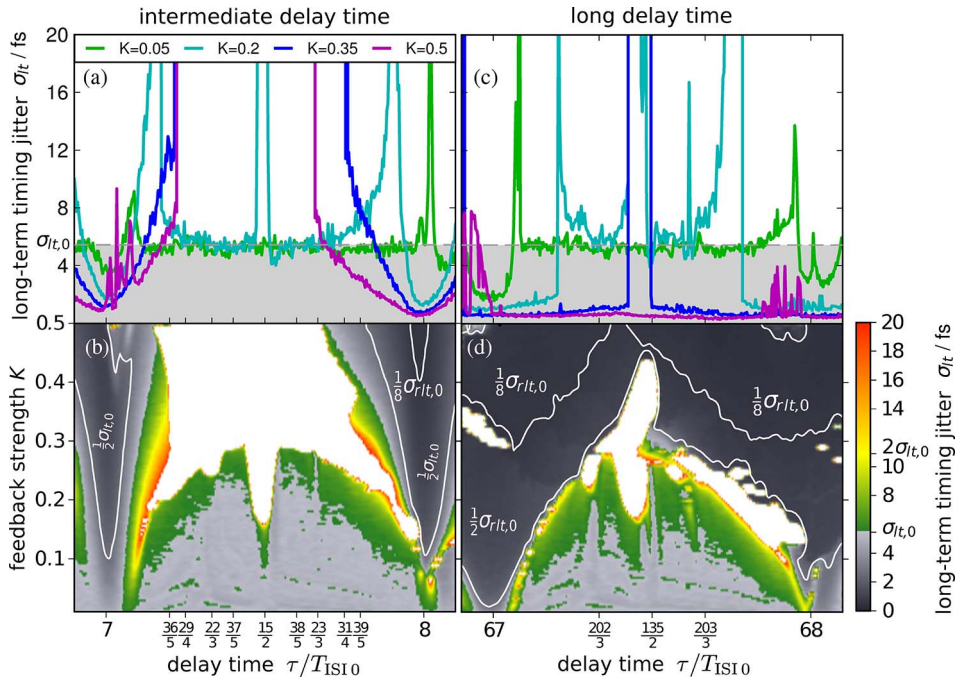

Fig. 9. Same as in Fig. 8 but for finite α-factors $\alpha_g = \alpha_q = 2$.

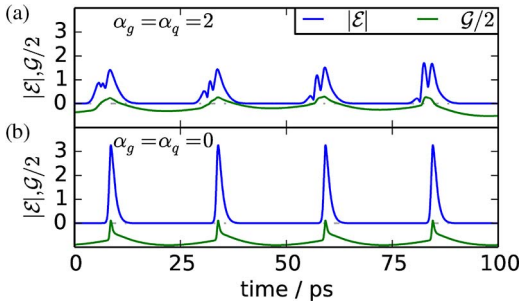

Fig. 10. Timeseries of the absolute value of the field amplitude $|\mathcal{E}|$ and the net gain $\mathcal{G}$ for the deterministic system subject to intermediate strength $(K = 0.3)$ resonant feedback $(\tau = 67\ T_{ISI,0})$ for $\alpha_g = \alpha_q = 2$ (a) and for zero α-factors (b). Parameters: D = 0, and other parameters as in Table 1.

resonances. In the case of long delay the resonance cones are wider and there is only a small region in K-τ space where the pulse stream is unstable.

In Fig. 9 the same plots are shown, however, this time for finite α-factors $\alpha_g = \alpha_q = 2$. We use moderate symmetric α-factors that were also used in [26] to model a hybrid ML QD laser. The most striking change caused by the inclusion of finite α-factors is the appearance of regions of unstable pulse streams close to the main resonances. This is in agreement with experiments by [20] and [27], where instabilities were observed for nearly resonant feedback.

Fig. 10 depicts timeseries of $|\mathcal{E}|$ and $\mathcal{G}$ at the 67th main resonance, with $K = 0.3$, for the deterministic system. For $\alpha_g = \alpha_q = 2$ (panel (a)) the time series is obtained within the region of unstable pulse streams also visible in white in Fig. 9. Comparing panels (a) and (b) of Fig. 10 reveals that for $\alpha_g = \alpha_q = 0$ the output is periodic, however for $\alpha_g = \alpha_q = 2$ the output is non-periodic and the pulses are deformed.

Significant reductions in the timing jitter can still be observed for high feedback strengths $(K > 0.2)$. This is especially true for long delay away from the main resonances (see the purple

line in Fig. 9(c)). These results are in good agreement with various experimental studies [7], [8], [20], [28]. In [7], close to two orders of magnitude reduction of the RF spectrum linewidth was reported for a semiconductor quantum well ML laser subject to optical feedback. In [8], measurements of the timing jitter of a quantum dot ML laser subject to optical feedback are reported for feedback delay times spanning one laser cavity roundtrip time. Suppression of the timing jitter was observed in resonance cones about resonant feedback delay times, corresponding well to our predictions.

6. Conclusion

We have compared three methods of calculating the rms timing jitter of a passively ML laser and shown that all three methods exhibit the same dependence on the delay time τ. We thereby validate the use of the computationally less expensive long-term timing jitter calculation method when dealing with passively ML lasers.

We find that when the α-factors in the gain and absorber sections are zero, the timing jitter is reduced by resonant feedback with respect to the solitary laser. In regions of non-resonant feedback an increase in the timing jitter can be observed. These increases with respect to the solitary laser are associated with switching events between bistable solutions or with a feedback induced deformation of the pulse shape leading to less stable pulse shapes. In the regime of long delay the main resonance cones are broadened and a greater reduction in the timing jitter is observed. For both intermediate and long delay times that are outside the main resonance cones, unstable pulse streams can be observed at large feedback strengths.

For finite α-factors we find that the resonance cones are largely preserved. However, regions of unstable pulse stream are found to occur on and near the main resonances. This relatively simple model therefore correctly predicts experimental occurrences [20], [27]. The strong dependence of the timing jitter on the amplitude-phase coupling suggests the need for further analysis of the impact of the amplitude-phase coupling on the ML laser output.

Acknowledgement

We would like to thank B. Lingnau and A. Vladimirov for fruitful discussions.

References

[1] E. A. Avrutin, J. H. Marsh, and E. L. Portnoi, "Monolithic and multi-gigahertz mode-locked semiconductor lasers: Constructions, experiments, models and applications," *Proc. Inst. Elect. Eng.—Optoelectron.*, vol. 147, no. 4, pp. 251–278, Aug. 2000.

[2] F. Lelarge *et al.*, "Recent advances on InAs/InP quantum dash based semiconductor lasers and optical amplifiers operating at 1.55 μm," *IEEE J. Sel. Top. Quantum Electron.*, vol. 13, no. 1, pp. 111–124, Jan./Feb. 2007.

[3] K. Lüdge, *Nonlinear Laser Dynamics—From Quantum Dots to Cryptography*, K. Lüdge, Ed. Weinheim, Germany: Wiley-VCH, 2012.

[4] M. Schell, A. Weber, E. Schöll, and D. Bimberg, "Fundamental limits of sub-ps pulse generation by active mode locking of semiconductor lasers: The spectral gain width and the facet reflectivities," *IEEE J. Quantum Electron.*, vol. 27, no. 6, pp. 1661–1668, Jun. 1991.

[5] D. J. Derickson, P. A. Morton, J. E. Bowers, and R. L. Thornton, "Comparison of timing jitter in external and monolithic cavity mode-locked semiconductor lasers," *Appl. Phys. Lett.*, vol. 59, no. 26, pp. 3372–3374, Dec. 1991.

[6] C. Y. Lin, F. Grillot, Y. Li, R. Raghunathan, and L. F. Lester, "Characterization of timing jitter in a quantum dot passively mode-locked laser at low offset frequency," in *Proc. 23rd Annu. Meet. IEEE Photon. Soc.*, 2010, pp. 361–362.

[7] O. Solgaard and K. Y. Lau, "Optical feedback stabilization of the intensity oscillations in ultrahigh-frequency passively modelocked monolithic quantum-well lasers," *IEEE Photon. Technol. Lett.*, vol. 5, no. 11, pp. 1264–1267, Nov. 1993.

[8] D. Arsenijević, M. Kleinert, and D. Bimberg, "Phase noise and jitter reduction by optical feedback on passively mode-locked quantum-dot lasers," *Appl. Phys. Lett.*, vol. 103, pp. 231101-1–231101-4, Dec. 2013.

[9] L. Drzewietzki, S. Breuer, and W. Elsäßer, "Timing phase noise reduction of modelocked quantum-dot lasers by time-delayed optoelectronic feedback," *Electron. Lett.*, vol. 49, no. 8, pp. 557–559, Apr. 2013.

[10] C. Otto, K. Lüdge, A. G. Vladimirov, M. Wolfrum, and E. Schöll, "Delay induced dynamics and jitter reduction of passively mode-locked semiconductor laser subject to optical feedback," *New J. Phys.*, vol. 14, no. 11, p. 113 033, Nov. 2012.

[11] J. Mulet and J. Mørk, "Analysis of timing jitter in external-cavity mode-locked semiconductor lasers," *IEEE J. Quantum Electron.*, vol. 42, no. 3, pp. 249–256, Mar. 2006.

[12] E. A. Avrutin and B. M. Russell, "Dynamics and spectra of monolithic mode-locked laser diodes under external optical feedback," *IEEE J. Quantum Electron.*, vol. 45, no. 11, pp. 1456–1464, Nov. 2009.
[13] H. Simos, C. Simos, C. Mesaritakis, and D. Syvridis, "Two-section quantum-dot mode-locked lasers under optical feedback: Pulse broadening and harmonic operation," *IEEE J. Quantum Electron.*, vol. 48, no. 7, pp. 872–877, Jul. 2012.
[14] C. Simos, H. Simos, C. Mesaritakis, A. Kapsalis, and D. Syvridis, "Pulse and noise properties of a two section passively mode-locked quantum dot laser under long delay feedback," *Opt. Commun.*, vol. 313, pp. 248–255, Feb. 2014.
[15] A. G. Vladimirov, D. Turaev, and G. Kozyreff, "Delay differential equations for mode-locked semiconductor lasers," *Opt. Lett.*, vol. 29, no. 11, pp. 1221–1223, Jun. 2004.
[16] A. G. Vladimirov and D. Turaev, "Model for passive mode locking in semiconductor lasers," *Phys. Rev. A, At. Mol. Opt. Phys.*, vol. 72, no. 3, pp. 033808-1–033808-13, Sep. 2005.
[17] C. Otto, *Dynamics of Quantum Dot Lasers—Effects of Optical Feedback and External Optical Injection*, ser. Springer Theses. Berlin, Germany: Springer-Verlag, 2014.
[18] D. von der Linde, "Characterization of the noise in continuously operating mode-locked lasers," *Appl. Phys. B*, vol. 39, no. 4, pp. 201–217, Apr. 1986.
[19] B. Kolner and D. Bloom, "Electrooptic sampling in GaAs integrated circuits," *IEEE J. Quantum Electron.*, vol. QE-22, no. 1, pp. 79–93, Jan. 1986.
[20] G. Fiol, M. Kleinert, D. Arsenijević, and D. Bimberg, "1.3 μm range 40 GHz quantum-dot mode-locked laser under external continuous wave light injection or optical feedback," *Semicond. Sci. Technol.*, vol. 26, no. 1, p. 014006, Jan. 2011.
[21] G. Fiol, "1.3 μm monolithic mode-locked quantum-dot semiconductor lasers," Ph.D. dissertation, Technische Univ. Berlin, Berlin, Germany, 2011.
[22] R. Rosales *et al.*, "InAs/InP quantum-dot passively mode locked lasers for 1.55 μm applications," *IEEE J. Sel. Top. Quantum Electron.*, vol. 17, no. 5, pp. 1292–1300, Sep./Oct. 2012.
[23] C. W. Gardiner, *Handbook of Stochastic Methods for Physics, Chemistry and the Natural Sciences*. Berlin, Germany: Springer-Verlag, 2002.
[24] D. C. Lee, "Analysis of jitter in phase-locked loops," *IEEE Trans. Circuits Syst. II*, vol. 49, no. 11, pp. 704–711, Nov. 2002.
[25] F. Kefelian, S. O'Donoghue, M. T. Todaro, J. G. McInerney, and G. Huyet, "RF linewidth in monolithic passively mode-locked semiconductor laser," *IEEE Photon. Technol. Lett.*, vol. 20, no. 16, pp. 1405–1407, Aug. 2008.
[26] G. Fiol *et al.*, "Hybrid mode-locking in a 40 GHz monolithic quantum dot laser," *Appl. Phys. Lett.*, vol. 96, no. 1, pp. 011104-1–011104-3, Jan. 2010.
[27] C. Y. Lin, F. Grillot, N. A. Naderi, Y. Li, and L. F. Lester, "rf linewidth reduction in a quantum dot passively mode-locked laser subject to external optical feedback," *Appl. Phys. Lett.*, vol. 96, no. 5, pp. 051118-1–051118-3, Feb. 2010.
[28] S. Breuer *et al.*, "Investigations of repetition rate stability of a mode-locked quantum dot semiconductor laser in an auxiliary optical fiber cavity," *IEEE J. Quantum Electron.*, vol. 46, no. 2, pp. 150–157, Feb. 2010.